Random hyperbolic graphs with arbitrary mesoscale structures

Stefano Guarino and Enrico Mastrostefano*
Istituto per le Applicazioni del Calcolo "Mauro Picone" (CNR-IAC), Via dei Taurini 19, Rome 00185, Italy

Davide Torre
ISI Foundation, Via Chisola 5, Turin 10126, Italy

(Received 19 August 2025; accepted 16 October 2025; published 12 November 2025)

Real-world networks exhibit universal structural properties such as sparsity, small worldness, heterogeneous degree distributions, high clustering, and community structures. Geometric network models, particularly random hyperbolic graphs (RHGs), effectively capture many of these features by embedding nodes in a latent similarity space. However, networks are often characterized by specific connectivity patterns between groups of nodes—i.e., communities—that are not geometric, in the sense that the dissimilarity between groups does not obey the triangle inequality. Structuring connections only based on the interplay of similarity and popularity thus poses fundamental limitations on the mesoscale structure of the networks that RHGs can generate. To address this limitation, we introduce the random hyperbolic block model (RHBM), which extends RHGs by incorporating block structures within a maximum-entropy framework. We demonstrate the advantages of RHBM through synthetic network analyses, highlighting its ability to preserve community structures where purely geometric models fail. Our findings emphasize the importance of latent geometry in network modeling while addressing its limitations in controlling mesoscale mixing patterns.

DOI: 10.1103/5q8n-lnc1

I. INTRODUCTION

Models of complex networks aim to replicate structural patterns observed in real-world systems while enabling effective network randomization for benchmarking and hypothesis testing [1–3]. Over the past few decades, numerous studies have identified a set of universal characteristics that most real-world networks share. These include sparsity [4], the small-world property [5], an inhomogeneous degree distribution [6] and a high clustering coefficient [7]. Most real networks, however, also exhibit nontrivial mesoscale structures, such as communities with specific mixing patterns [8]. Defining network models that provide explicit control of statistics at all scales is crucial for realistic network representations [9,10].

Random hyperbolic graphs (RHG) provide a compelling framework to explain various observed network characteristics by embedding nodes in a hidden metric space with negative curvature [7,11–14]. Such a latent geometry provides a powerful approach to modeling networks, structuring connections based on both similarity and popularity [15–17]. In the $\mathbb{S}^D$ model, node popularity is controlled by latent degrees κ_i and similarity by node-to-node distances $x_{ij} = R\Delta\theta_{ij}$ within a D-dimensional sphere. The edge probability reads

$$p_{ij} = \frac{1}{1 + \left(\frac{x_{ij}}{(\mu\kappa_i\kappa_j)^{1/D}}\right)^{\beta}}, \tag{1}$$

where the inverse temperature β controls the clustering coefficient, whereas the density parameter μ ensures the correct average degree.

The hidden degrees in $\mathbb{S}^D$ can be mapped onto radial coordinates in a hyperbolic plane $\mathbb{H}^{D+1}$, transforming the spherical representation with hidden degrees into a purely geometric hyperbolic one. When hidden degrees follow a power-law distribution with exponent $\gamma \geqslant 2$, the $\mathbb{S}^D$ and $\mathbb{H}^{D+1}$ models become isomorphic in the thermodynamic limit [11]. The popularity-similarity optimization (PSO) model [18] and its nonuniform generalization (nPSO) [19] extend the ideas of RHG by incorporating dynamic elements that reflect the balance between popularity and similarity in the emergence of real networks. Despite the conceptual elegance of hyperbolic spaces and the potential benefits of higher dimensions ($D > 1$), the $\mathbb{S}^1$ model remains the most widely used due to its simplicity. It is characterized by two fundamental properties: (i) when angular coordinates are uniformly distributed, the expected degree of a vertex converges to its hidden degree in the limit of large networks, $\langle \deg_i \rangle_{\mathbb{S}^1} \to \kappa_i$; and (ii) clustering decreases as $\beta \to 1$ and stabilizes at a constant for $\beta \to +\infty$.

Hyperbolic latent spaces naturally capture hierarchical and transitive structures, mirroring empirical properties such as degree heterogeneity and clustering [12,19,20]. A fundamental limitation of these models, however, is their lack of explicit control over mixing patterns at intermediate scales. Both RHG and PSO models can produce networks with strong communities [13,21,22], but these arise implicitly rather than as a controlled feature. Modularity can be imposed via angular-node aggregation [15,19,20,23], but intercommunity connectivity is entirely driven by similarity in the latent space.

This limitation highlights a fundamental challenge for latent-space models whenever mesoscale structures arise from categorical or sharply modulated attributes. While geometric proximity effectively captures smooth, similarity-driven

*Contact author: enrico.mastrostefano@cnr.it

connectivity based on ordinal or scalar attributes [21,22,24,25], it cannot easily represent patterns where link probability increases, decreases, or changes abruptly with attribute distance. The max-entropy derivation of hyperbolic models constrains link probability to be a continuous and monotonic function of geometric distance, making it unclear how—or whether it is even feasible—to map attributes and attribute distances into geometric patterns that faithfully reproduce the intended connectivity structure. For instance, age-based social mixing involves both a strong diagonal (same-age contacts) and strong parent-child subdiagonals: individuals should be geometrically close to both their peers and to parents or children, yet these groups have no reason to be proximate—violating the triangle inequality. Similarly, three political parties may coexist such that one acts as an intermediary collaborating with both others, while the latter two remain strongly antagonistic; in such cases, collaboration frequency may not follow any hypothetical ideological axis, producing arrangements incompatible with metric embeddings. Coexpression networks display analogous behavior, where modular patterns arise from pathway membership rather than proximity in expression space.

Beyond categorical or modular structure, many systems also exhibit complementarity-driven connectivity, where links form between nodes with functionally matching but dissimilar attributes. Examples include protein–protein interactions, semantic relations, and collaboration or production networks, where complementarity and similarity often coexist. Such mechanisms generate patterns, typically quadrangular or bipartite motifs rather than triangles, that purely geometric models may fail to capture [26–28].

Increasing the dimensionality of latent hyperbolic spaces has been suggested as a way to enable finer control over group interactions and overcome the intrinsic correlations between node distances found in low dimensions [29–32]. On the other hand, the maximum clustering coefficient that can be obtained from a geometric model decreases as the dimension of the space increases [33]. Existing models lack mechanisms for leveraging dimensionality to enforce specific community-mixing patterns while preserving essential network properties. Whether arbitrary group-mixing patterns are compatible with a popularity-similarity framework is yet to be clarified in the literature.

In this paper, we propose the *random hyperbolic block model* (RHBM), a generalization of RHGs that incorporates explicit control over the network's mixing matrix by means of a set of hidden forces binding node groups. Instead of hidden degrees, we introduce a hidden fitness parameter, normalized according to block connectivity. We show that the RHBM, as the $\mathbb{S}^1$ model [34], can be interpreted as an entropy-maximizing probabilistic mixture of grand-canonical network ensembles. This means that the proposed formulation is optimal for geometric networks with constrained expected-degree sequence and group-mixing matrix.

We demonstrate that the RHBM can be equivalently represented as the union of $\binom{n}{2}$ $\mathbb{S}^1$ graphs, corresponding to intra- and interblock connections among n communities, provided that node-latent features are drawn once and applied consistently across subgraphs, ensuring stable centrality and homophily patterns. Due to this equivalence, we introduce the alternative notation $(\mathbb{S}^1)^{\binom{n}{2}}$ for this graph model.

To highlight its relevance, we present experimental results in support of the intuition that attribute-based group mixing is, in general, nongeometric. We generated synthetic networks using the RHBM and embedded them in $\mathbb{S}^D$, for $D = 1, \ldots, 5$, using the state-of-the-art tool D-Mercator [23]. In D-Mercator, the algorithm infers the inverse temperature β, the parameter μ controlling the network's average degree, the radius of the $\mathbb{S}^D$ disk, the hidden degrees, and the latent angular coordinates, maximizing the likelihood of the inferred latent coordinates given the observed graph. By analyzing the graphs obtained from the embedding, we show that models based solely on the popularity-similarity paradigm can capture local properties such as degree distributions and clustering but fail to enforce specific mesoscale structures like community mixing. Even the choice of model parameters and latent coordinates that best explain the input network, in fact, fails to explain the input mixing patterns, regardless of D. In summary, we show that our proposed RHBM, by explicitly incorporating block-level constraints, permits to regulate community structures and mixing patterns while maintaining the fundamental strengths of hyperbolic network models. Our findings challenge the notion that purely geometric models suffice to explain real-world network structures.

II. THE RANDOM HYPERBOLIC BLOCK MODEL

The RHBM extends the $\mathbb{S}^1/\mathbb{H}^2$ models by addressing the case in which the N nodes are organized into n disjoint *blocks* (or *communities*), whose connectivity patterns are controlled by a symmetric matrix $\Phi = \{\Phi_{IJ}\}$ of latent forces [35]. As in the $\mathbb{S}^1$ model, the nodes are placed uniformly at random on a disk of radius R assigning angular coordinate $\theta_i \in [0, 2\pi)$ to node i. Instead of a hidden degree, each node has a (hidden) fitness ϕ_i drawn from a suitable distribution. In the following, we will assume power-law-distributed fitness with exponent $\gamma = 2.5$, but any distribution is potentially usable. The probability per link reads

$$p_{ij} = \frac{1}{1 + \left(\frac{x_{ij}}{\tilde{\mu}_{IJ}\phi_i\phi_j\Phi_{IJ}}\right)^{\beta}}, \tag{2}$$

where $i \in I$, $j \in J$, $x_{ij} = R\Delta\theta_{ij}$, and $\tilde{\mu}_{IJ} = R\beta\sin(\pi/\beta)$. If we denote $\kappa_{iJ} = \phi_i\Phi_{IJ}$ the expected degree of i towards block J—i.e., the number of nodes in block J to which i is connected—and $\mu_{IJ} = \frac{\tilde{\mu}_{IJ}}{\Phi_{IJ}}$, Eq. (2) can be rewritten as

$$p_{ij} = \frac{1}{1 + \left(\frac{x_{ij}}{\kappa_{iJ}\kappa_{jI}\mu_{IJ}}\right)^{\beta}}. \tag{3}$$

This shows that in the RHBM p_{ij} takes the same functional form of Eq. (1), with the only difference that the total hidden degrees κ_i, κ_j and the normalization constant μ are replaced by their blockwise counterparts κ_{iJ}, κ_{jI}, and μ_{IJ}.

A. Maximum-entropy formulation

In the thermodynamic limit $N \to \infty$, the RHBM can be defined as the maximum-entropy ensemble P satisfying

$$\langle E \rangle_P = W, \tag{4}$$

$$\langle L_{IJ}\rangle_P = F_{IJ} \quad \text{for all } I, J, \tag{5}$$

$$\langle \deg_i\rangle_P = f_i \sum_J F_{i_J} \quad \text{for all } i. \tag{6}$$

Equation (4) binds the expected total energy $E = \sum_{ij} \varepsilon(x_{ij})$ to W, Eq. (5) sets the expected number of links between blocks I and J (or twice that number if $I = J$) to F_{IJ}, and Eq. (6) controls the expected degree sequence of the network. The consistency of Eqs. (5) and (6) is guaranteed by taking f_i so that $\sum_{i\in I} f_i = 1$ for all I. f_i can thus be interpreted as the fraction of all edges incident on block I that are incident on node i.

As for the standard $\mathbb{S}^1$ model, the maximum-entropy probability per graph factorizes in terms of independent probabilities per link as

$$p_{ij} = \frac{1}{1 + e^{\lambda_i+\lambda_j+\eta_{IJ}+\beta\varepsilon(x_{ij})}},$$

where $i \in I$, $j \in J$, and β, η_{IJ} and λ_i are the Lagrange multipliers associated, respectively, to conditions Eqs. (4)–(6). Also, with the same line of reasoning used in Ref. [34], it can be proved that taking $\varepsilon(x_{ij}) = \ln(x_{ij})$ is the only way to suppress nonstructural degree correlations. This leads to

$$p_{ij} = \frac{1}{1 + \left(x_{ij} e^{\frac{\lambda_i+\lambda_j+\eta_{IJ}}{\beta}}\right)^\beta}. \tag{7}$$

For fixed λ_i and η_{IJ} (i.e., fixed f_i and F_{IJ}), the expected probability that nodes i and j are connected can be found integrating p_{ij} over θ_j and λ_j. In the limit $N \to \infty$ one obtains

$$\langle p_{ij} \mid \lambda_i, \eta_{IJ}\rangle = \frac{1}{\tilde{\mu}_{IJ}} e^{-\frac{\eta_{IJ}}{\beta}} e^{-\frac{\lambda_i}{\beta}} \langle e^{-\frac{\lambda}{\beta}}\rangle. \tag{8}$$

Further integrating Eq. (8) over λ_i gives

$$e^{-\frac{\eta_{IJ}}{\beta}} = \frac{\tilde{\mu}_{IJ} F_{IJ}}{N_I N_J} \frac{1}{\langle e^{-\frac{\lambda}{\beta}}\rangle^2}, \tag{9}$$

$$e^{-\frac{\lambda_i}{\beta}} = f_i N_I \langle e^{-\frac{\lambda}{\beta}}\rangle, \tag{10}$$

which, plugged into Eq. (7), give

$$p_{ij} = \frac{1}{1 + \left(\frac{x_{ij}}{\tilde{\mu}_{IJ} f_i f_j F_{IJ}}\right)^\beta}. \tag{11}$$

Equation (11) shows that this maximum-entropy approach yields exactly the model defined by Eq. (2), provided that $\phi_i = f_i$ and $\Phi_{IJ} = F_{IJ}$—i.e., that the latent fitness equals the block-normalized degree, and that the hidden force between two blocks equals the expected number of edges between them. Let us underline that the equivalence works with exactly $\phi_i = f_i$ and $\Phi_{IJ} = F_{IJ}$ only in the thermodynamic limit $N \to \infty$. In a finite system, the values for ϕ_i and Φ_{IJ} that satisfy Eqs. (5) and (6) for given f_i and F_{IJ} must be found numerically. A more detailed derivation is given in the Appendixes.

B. Alternative formulation: $(\mathbb{S}^1)^{\binom{n}{2}}$

The RHBM can be equivalently obtained under the following system of *stronger* constraints [36]

$$\langle E\rangle_P = W, \tag{12}$$

$$\langle \deg_{iJ}\rangle_P = f_i F_{IJ} \quad \text{for all } i, J, \tag{13}$$

where $\deg_{iJ}$ is the degree of i towards J. Equation (13), which implies both Eqs. (5) and (6), states that f_i, instead of just controlling i's expected total degree, controls i's expected degree towards each and every blocks in the graph. The inverse—Eqs. (5) and (6) implying Eq. (13)—is not true in general, but it is true under the maximum-entropy principle, because the least-restrictive assumption one can make is that the popularity of a node does not vary from one block to another. It is easy to verify that a model defined in terms of Eqs. (12) and (13) is equivalent to the union of the $\binom{n}{2}$ graphs obtained imposing

$$\langle E_{IJ}\rangle_P = W_{IJ}, \tag{14}$$

$$\langle \deg_{iJ}\rangle_P = f_i F_{IJ} \quad \text{for all } i \in I, \tag{15}$$

$$\langle \deg_{jI}\rangle_P = f_j F_{IJ} \quad \text{for all } j \in J, \tag{16}$$

for all possible choices of I, J, and suitable W_{IJ}, where conditions Eqs. (14)–(16) define a bipartite graph if $I \neq J$. In particular, this implies that the $\mathbb{S}^1$ model can be generalized to accommodate a community structure by simply considering each subgraph defined by a pair (I, J) as a mono/bipartite $\mathbb{S}^1$ graph, provided that (i) the hidden degrees are replaced with block-normalized hidden fitnesses; (ii) both the hidden fitness ϕ_i and the latent angular coordinate θ_i associated to vertex i are drawn just once and for all—i.e., not redrawn for each subgraph. The fact that node i has the same ϕ_i in all subgraphs guarantees that Eq. (6) holds and that the graph has, in good approximation, the desired degree distribution. On the other hand, the fact that i has the same θ_i in all subgraphs preserves the transitivity of the vertex similarity across different subgraphs, so as to guarantee the desired high clustering for the entire network. We emphasize that, while the subgraphs share the same latent coordinates for all nodes and are therefore not statistically independent, the edge densities of different subgraphs can be controlled independently through the mixing matrix, that modulates the expected connectivity between and within groups.

III. EXPERIMENTS

To assess the expressive power and limitations of the RHBM, we conducted a series of controlled experiments, aimed at testing how well a purely geometric embedding—specifically, the one produced by D-Mercator—can recover key structural properties of synthetic networks generated with the model.

A. Experimental setup

The base parameters of the RHBM are
(1) N: number of nodes,
(2) k: average degree,

(3) γ: exponent of the power-law degree/fitness distribution,

(4) β: inverse temperature,

(5) n: number of communities.

We have set the mixing matrix F using a parametric model that allows us to consider a variable range of mixing patterns:

$$F(q, \rho, n) = (1 + \rho)\frac{I}{n} + (1 - \rho)\frac{T_q}{\sum_{ij}[T_q]_{ij}}, \qquad (17)$$

where I is the identity matrix and T_q is a Toeplitz matrix with $[T_q]_{ii} = 0$ for all i and $[T_q]_{ij} = q^{|i-j|}$ for all $i \neq j$. The parameter $\rho \in [-1, 1]$ interpolates between disassortative and assortative mixing, while $q \in (0, 1]$ controls the decay of connectivity away from the diagonal, making it possible to obtain ordered community structures. The matrices generated by this model capture a range of realistic structural patterns that, albeit clearly not exhaustive, provide a meaningful approximation of mixing behaviors that can occur in real systems. It is worth mentioning that the parameters ρ and q used in the experiments have not been deliberately chosen in a way that would produce ill-defined matrices or compromise D-Mercator's operating principles. To clarify this point, more details on the model and a visualization of the matrices used in the experiments can be found in the Appendixes.

We generated networks using the RHBM, varying one parameter at a time from the sets $N \in \{1000, 3000, 5000\}$, $k \in \{5, 10, 20\}$, $n \in \{2, 10, 100\}$, $\rho \in \{-0.5, 0, 0.5\}$, $q \in \{0.5, 0.75, 1\}$, $\beta \in \{2, 5, 10\}$, while keeping all others fixed at $N = 3000$, $k = 10$, $\gamma = 2.5$, $n = 10$, $\rho = 0.5$, $q = 1$ $\beta = 2$. Each generated network was embedded using D-Mercator, varying the latent space dimension $D \in \{1, 2, 3, 4, 5\}$. From each embedding, we computed

(i) The expected mixing matrix (based on the edge probability formula in the $\mathbb{S}^D$ model),

(ii) The expected degree sequence,

(iii) Ten synthetic networks sampled from the inferred edge probabilities, used to compute global and average local-clustering coefficients.

B. Results and discussion

(a) Model validation. For each parameter configuration, we generated 10 independent RHBM graphs and summarize the results in Fig. 1. The degree complementary cumulative distribution functions (CCDFs) (a) exhibit the expected heavy-tailed behavior induced by the imposed fitness distribution. Global and average local clustering (b)–(c), reported with standard-deviation error bars across runs, remain well above the Erdös-Rényi baseline; in particular, the global clustering is $\approx 20\times$ the graph density, indicating nontrivial transitivity. The realized block mixing (d) closely matches the imposed matrix, with relative error typically within a few percent. Taken together, these results confirm that the model behaves as designed and enforces both microscopic and mesoscale constraints.

(b) Block mixing-matrix reconstruction. To evaluate the accuracy of mixing-matrix reconstruction, we computed the relative absolute error:

$$\frac{\|F_{\text{out}} - F_{\text{in}}\|_1}{\|F_{\text{in}}\|_1},$$

where F_{in} is the ground-truth input matrix and F_{out} the one expected from the embedding. The results (Fig. 2) show that the error is generally significant, ranging from 10%–15% up to 50%–55%. Errors tend to be lower for smaller networks, fewer communities, more disassortative or orderly mixing patterns, and higher embedding dimensions.

(c) Degree sequence reconstruction. We compared the expected degree sequence derived from the embedding with the one of the input RHBM graph. As shown in Fig. 3, the match is nearly perfect across all tested configurations, confirming that D-Mercator captures node popularity extremely well.

(d) Clustering coefficient. We computed the relative error in both the global and average local clustering coefficients:

$$\frac{|C - C_{\text{in}}|}{C_{\text{in}}}.$$

Figures 4 and 5 show that the error is consistently low—below 20%–30% in all cases. Local clustering is best preserved for $D = 1$, while global clustering shows slightly better fidelity for $D = 1$ and $D = 5$, without major differences across parameter settings.

(e) Discussion. Overall, the results suggest that D-Mercator embeddings of networks generated with the RHBM are highly effective at preserving local structural properties such as node degrees and clustering, even under diverse parameter regimes. However, they fall short of recovering mesoscopic structures such as group-to-group connectivity patterns, indicating that purely geometric representations may not suffice to explain intermediate-scale structure when group mixing is imposed independently of geometry.

IV. CONCLUSION

Intermediate-scale structures, such as communities, are a typical feature of real-world networks with a significant impact on their functionality and dynamics. Identifying what constitutes a community is often challenging, therefore, when creating synthetic networks, it is essential to reproduce specific connectivity patterns between nodes. Similarly, when developing a null model to abstract and analyze an existing network, it is critical to preserve these mesoscale structures, which are characterized by groups of nodes that are either densely connected internally or to each other.

In this article, we introduce the random hyperbolic block model, an extension of the $\mathbb{S}^1$ random geometric graph that allows for explicit control over the frequency of connections between different groups of nodes. Like the $\mathbb{S}^1$ model, the RHBM can be derived from an entropy-maximization principle, but with an additional set of constraints on the expected mixing matrix between communities. This formulation extends latent geometry models by incorporating an explicit and tunable mechanism for controlling intergroup connectivity, addressing a key limitation of purely geometric approaches where mesoscale structures arise only as an implicit consequence of node similarity.

The common approach used in the literature to enforce a community structure in $\mathbb{S}^D$ was using a different spatial distribution for each block of nodes [15,19,20,23]. In particular, spatial aggregation of nodes in the same community leads to assortative mixing, where intrablock edges are more likely

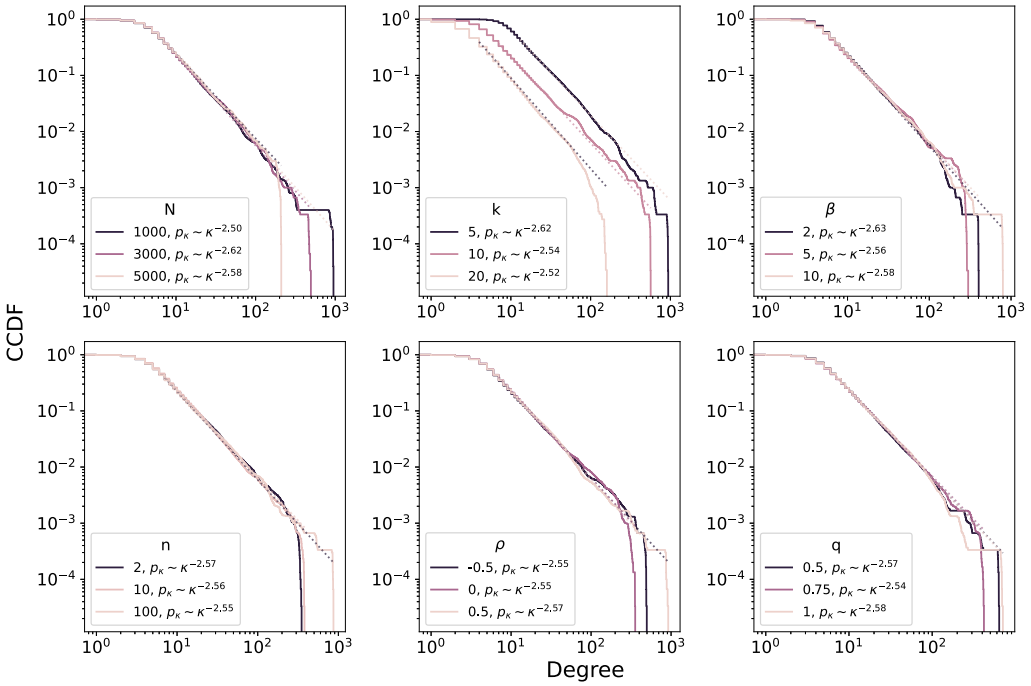

(a) Degree CCDF, with dotted power-law fit.

N	k	β	n	ρ	q	global clustering	avg. local clustering	rel. mixing error
1000	10	2	10	0.5	1.00	0.124 ± 0.002	0.483 ± 0.006	0.024 ± 0.003
3000	5	2	10	0.5	1.00	0.086 ± 0.002	0.307 ± 0.004	0.021 ± 0.003
3000	10	2	2	0.5	1.00	0.070 ± 0.001	0.470 ± 0.005	0.003 ± 0.001
3000	10	2	10	-0.5	1.00	0.068 ± 0.001	0.461 ± 0.004	0.016 ± 0.002
3000	10	2	10	0.0	1.00	0.085 ± 0.001	0.377 ± 0.005	0.016 ± 0.002
3000	10	2	10	0.5	0.50	0.087 ± 0.001	0.412 ± 0.003	0.014 ± 0.001
3000	10	2	10	0.5	0.75	0.087 ± 0.001	0.416 ± 0.002	0.013 ± 0.002
3000	10	2	10	0.5	1.00	0.079 ± 0.007	0.422 ± 0.028	0.014 ± 0.002
3000	10	2	100	0.5	1.00	0.092 ± 0.001	0.457 ± 0.005	0.024 ± 0.002
3000	10	5	10	0.5	1.00	0.118 ± 0.001	0.533 ± 0.002	0.009 ± 0.001
3000	10	10	10	0.5	1.00	0.136 ± 0.001	0.542 ± 0.003	0.007 ± 0.001
3000	20	2	10	0.5	1.00	0.106 ± 0.001	0.462 ± 0.002	0.009 ± 0.001
5000	10	2	10	0.5	1.00	0.058 ± 0.000	0.409 ± 0.003	0.010 ± 0.001

(b) Mean and standard deviation of the global clustering, average local clustering and relative mixing error. The reference configuration is gray boxed.

FIG. 1. Validation of the RHBM. We performed a one-variable-at-a-time analysis from a reference configuration with $N = 3000$, $k = 10$, $\beta = 2, n = 10, \rho = 0.5, q = 1$. The statistics are obtained from 10 independent graph instances. Panel (a) shows the complementary cumulative distribution function (CCDF) of the degree, obtained considering all nodes across the 10 graphs. Panel (b) shows the mean and standard deviation, across the 10 graphs, of the global clustering coefficient, the average local clustering coefficient, and the relative error between the imposed and realized mixing matrices.

than interblock ones. Due to the triangle inequality, however, one cannot have strong connectivity between both pairs of blocks (I, M) and (M, J) without also having non-negligible connectivity between (I, J), unless one allows very large variances that reduce the meaning of group structure. In addition, the nodes being uniformly distributed in the latent space is one key assumption of the $\mathbb{S}^D$ model, that guarantees node homogeneity and makes the model analytically treatable.

The RHBM addresses this issue decoupling attribute-based group mixing and individual popularity/similarity-based mixing.

We conducted a series of experiments to assess whether networks created with the RHBM have a more natural interpretation. To this end, we fed graphs obtained with the RHBM to the D-Mercator algorithm, the state-of-the-art model for multidimensional embeddings in $\mathbb{S}^D$, varying the latent-space dimension D. D-Mercator does not explicitly attempt at reconstructing the input attribute-based mixing, but it tries to identify the most suitable geometric representation for that network, given the observed connectivity patterns. By letting the input network change in aspects like the number of communities and the type of mixing, we verified that even the

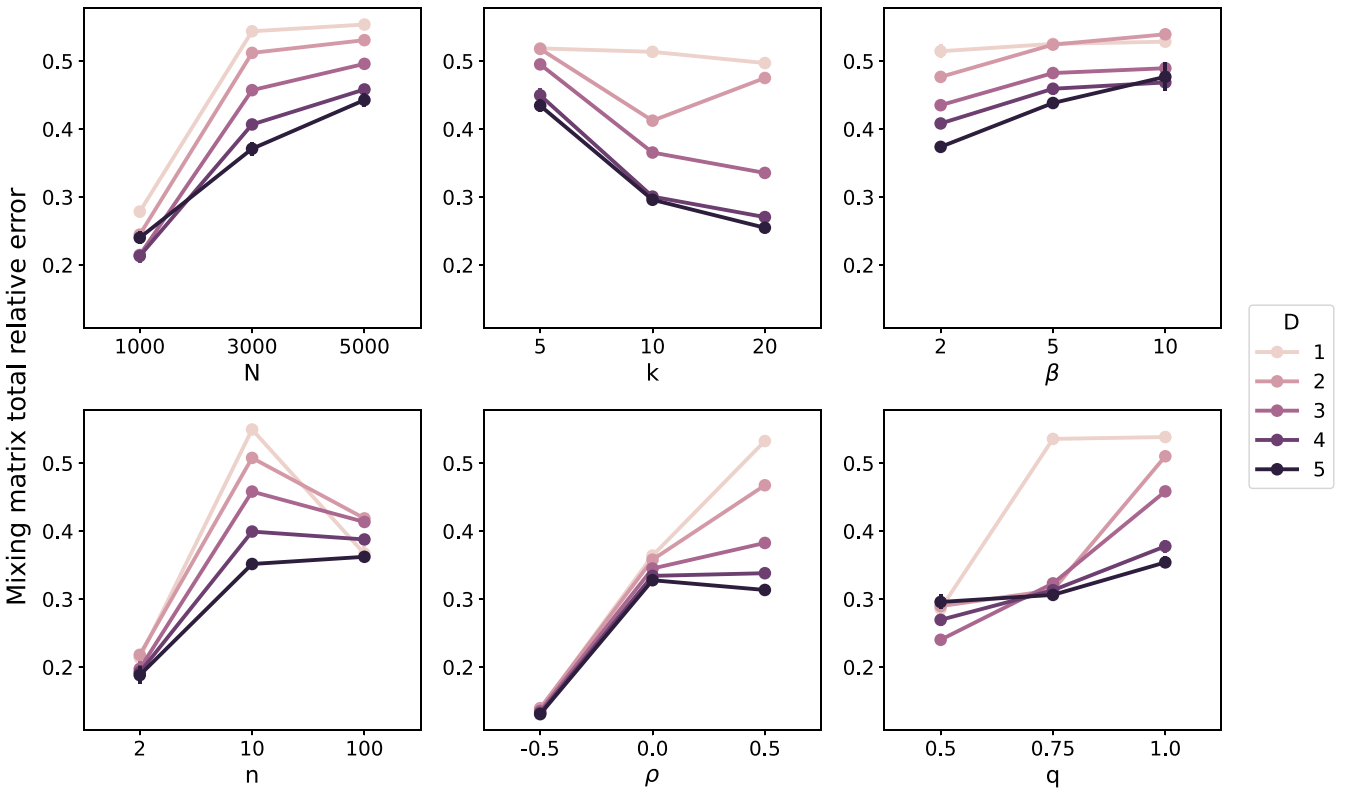

FIG. 2. Relative error in recovering the mixing matrix for various model configurations and embedding dimensions.

most plausible geometric configuration is generally insufficient to fully explain or reproduce the input intermediate-scale patterns. These results suggest that the RHBM offers a principled and flexible framework to model structured networks where community structure and geometric organization coexist, without artificially coupling the two.

In line with this view, prior studies observe a systematic tendency for similarity-driven interactions to close triads—hence more triangles—because neighbors of a node are likely to be similar to each other, whereas complementarity often yields rolelike or bipartite patterns in which two dissimilar sets connect to each other but not within themselves, producing more quadrangles (4-cycles) and related substructures [26–28]. These motif tendencies have been reported across domains (e.g., semantic relations, collaboration, and production links), and are compatible with our aim of separating geometric proximity from explicit control of intergroup connectivity.

An important consideration is whether networks generated by our model could be considered "geometric" under alternative definitions of clustering or network geometry. While our construction decouples traditional geometric clustering from community mixing patterns, it remains possible that different geometric frameworks, employing alternative notions of similarity or clustering, might capture both features simultaneously. Investigating such alternative geometric representations constitutes a promising avenue for future research.

Another critical step forward would be the application of an inference framework to fit the model's parameters to real-world network data, transforming the RHBM from a generative model into an analytical tool. Such an approach, which could be inspired by or adapted from principled Bayesian inference methods [37], would allow to test whether the combined geometric and community constraints of the RHBM provide a more accurate description of empirical data than simpler models and unlock its potential for empirical applications, such as community-aware network embedding or generative modeling of attributed graphs. We also plan to investigate the use of the RHBM as a randomization tool for real networks, generating synthetic graphs that preserve both the latent geometry and the mesoscale mixing patterns of the original while allowing controlled perturbation of finer topological details, thus enabling controlled null models for hypothesis testing. Future directions include a deeper exploration of the interplay between geometry and group mixing in dynamic or temporal settings, where connection patterns evolve over time.

While the model is referred to as *hyperbolic* due to the isomorphism between the $\mathbb{S}^1$ and $\mathbb{H}^2$ models, the current formulation has been developed in Euclidean space for analytical convenience. A natural next step is to explicitly formulate and analyze the RHBM directly in hyperbolic space, aligning its geometric underpinnings with the growing body of work in hyperbolic network science and potentially enhancing its descriptive power for hierarchical and treelike structures.

DATA AVAILABILITY

The data and the source code implementing the model that support the findings of this article are openly available [38].

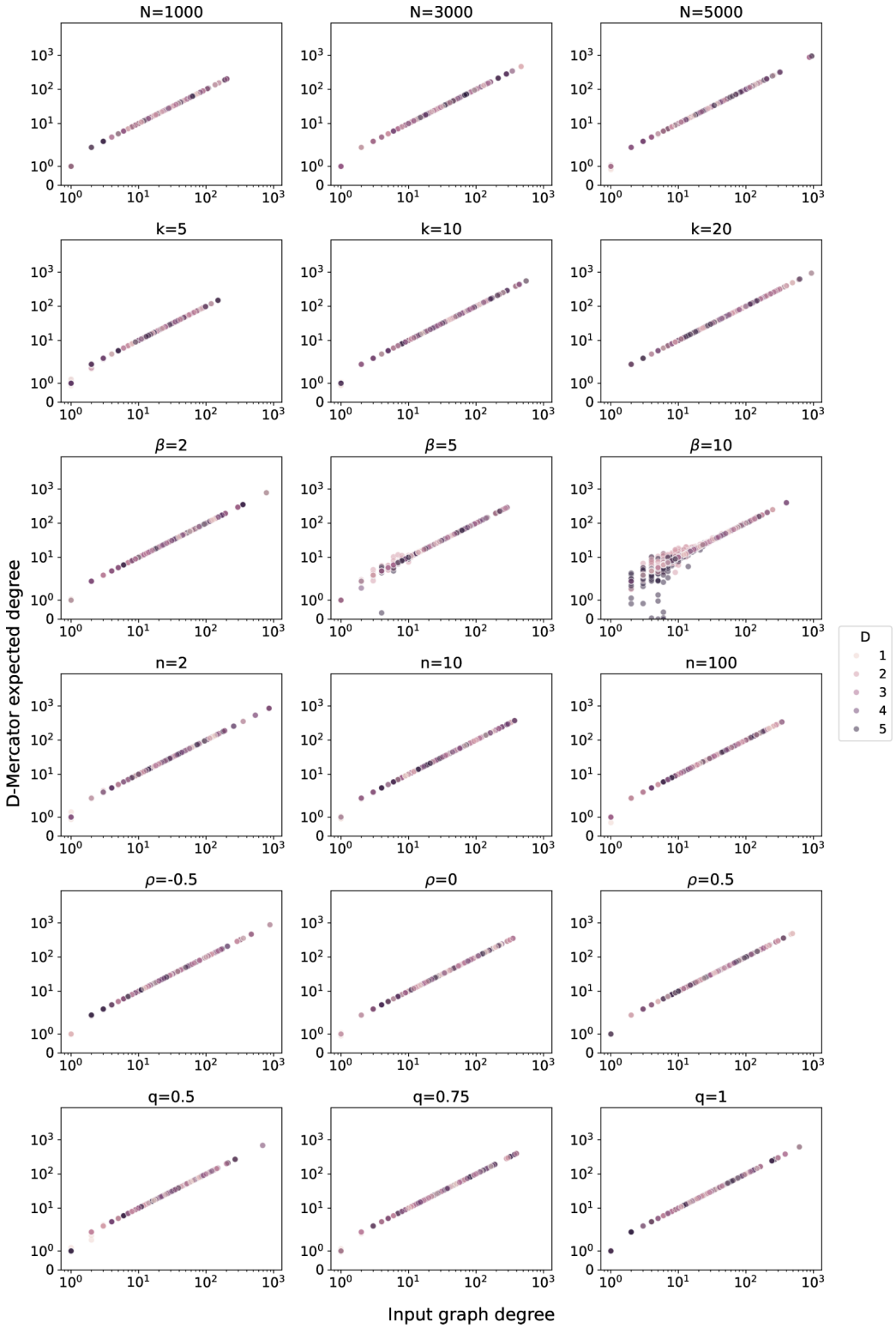

FIG. 3. Scatter plot of input vs reconstructed degree sequences. All points lie close to the identity line.

APPENDIX A: GEOMETRIC MODELS

The $\mathbb{S}^1$ model

The most elegant way to define the $\mathbb{S}^1$ model is through the formalism of entropy-based models. Let $\Delta(\theta_i, \theta_j) = (\pi - |\pi - |\theta_i - \theta_j||)$ denote the absolute angular distance between the latent coordinates θ_i and θ_j. For fixed R, let $x_{ij} = x(\theta_i, \theta_j) = R\Delta(\theta_i, \theta_j)$ be the distance between v_i and v_j on the $\mathbb{S}^1$ ring of radius R, and let $\varepsilon_{ij} = \varepsilon(x_{ij})$ be the *energy* of edge (i, j). By constraining the expected energy

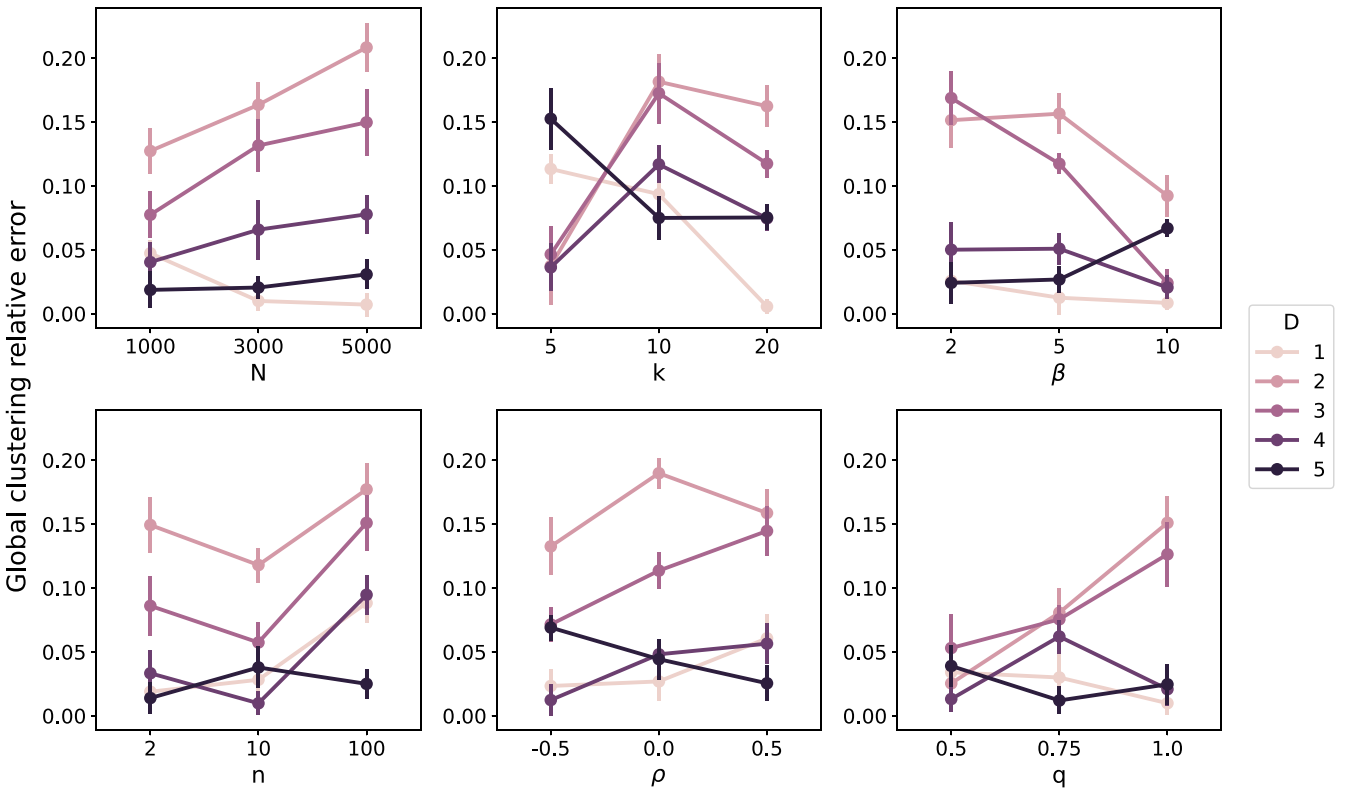

FIG. 4. Relative error in global-clustering coefficients. D-Mercator preserves clustering well across all configurations.

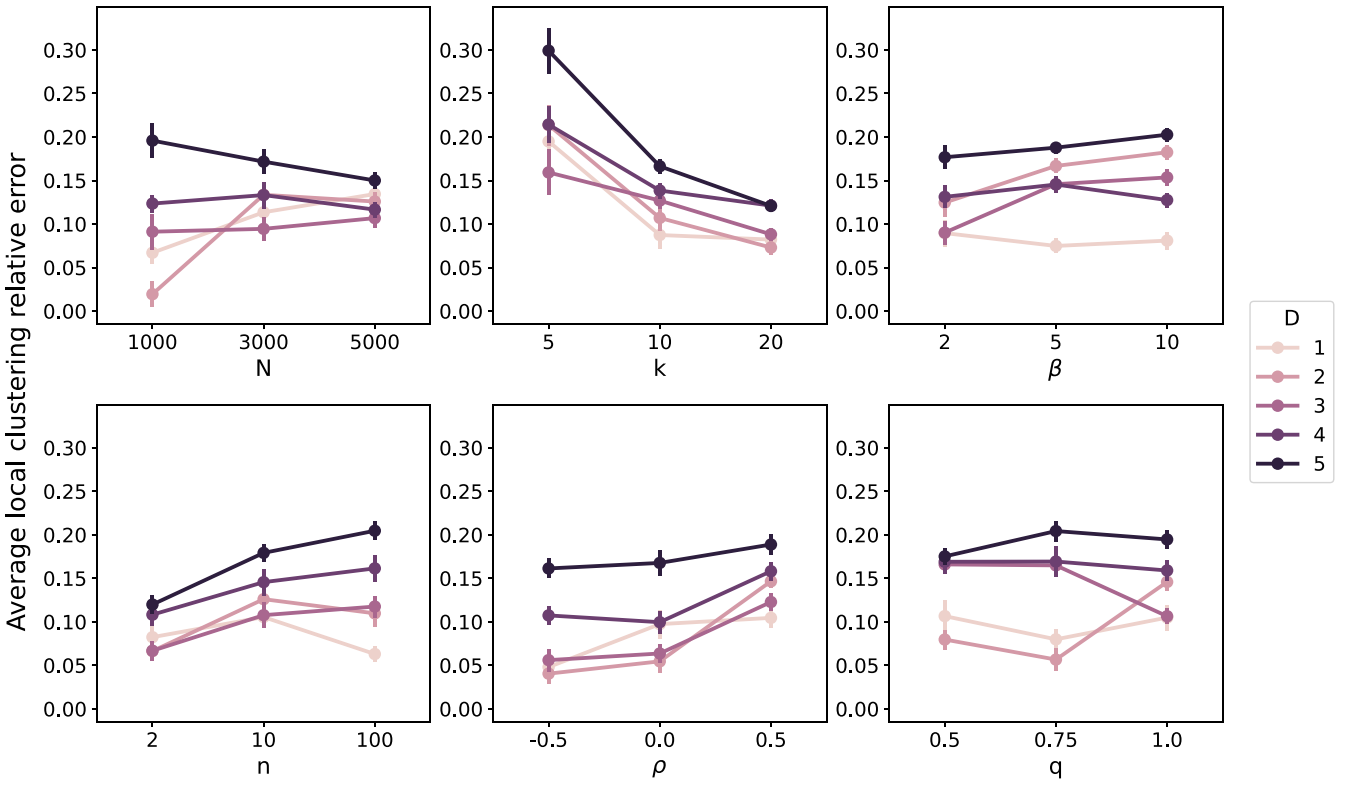

FIG. 5. Relative error in average local-clustering coefficients. Again, D-Mercator preserves clustering well across all configurations.

$E(G) = \sum_{i<j} \varepsilon_{ij} a_{ij}(G)$ of the system and the expected degree sequence, one obtains

$$\langle E \rangle_P = E^*, \tag{A1}$$

$$\langle \deg_i \rangle_P = \kappa_i^*. \tag{A2}$$

In Eqs. (A1) and (A2) the expectation is taken with respect to just the graph probability P, assuming that all latent coordinates are known. The maximum-entropy condition leads to a grand-canonical ensemble where the probability per graph factorizes in terms of probabilities per link as

$$p_{ij} = \frac{1}{1 + e^{\lambda_i + \lambda_j + \beta \varepsilon_{ij}}}, \tag{A3}$$

where β and λ_i are the Lagrange multipliers associated, respectively, to conditions Eqs. (A1) and (A2).

If the latent coordinates are drawn randomly with probability density functions $\rho(\theta)$ and $\rho(\kappa)$, conditions Eqs. (A1) and (A2) define a hyper-grand-canonical ensemble, i.e., a probabilistic mixture of the grand-canonical ensembles defined above. In this context, to suppress any nonstructural degree correlations, one must take $\varepsilon_{ij} = \ln(x_{ij})$ [34], so that p_{ij} can be rewritten as

$$p_{ij} = \frac{1}{1 + \left(x_{ij} e^{\frac{\lambda_i + \lambda_j}{\beta}}\right)^\beta}. \tag{A4}$$

If the nodes are placed uniformly at random on the $\mathbb{S}^1$ ring, then $\rho(\theta) = \frac{1}{2\pi}$ and the density of nodes on $\mathbb{S}^1$ is $\delta = \frac{N}{2\pi R}$. Without loss of generality, one can take $\theta_i = 2\pi$ so that $\Delta(\theta_i, \theta_j) = \theta_j$. By integrating over θ_j and λ_j, one obtains

$$\begin{aligned} \langle p_{ij} \mid \lambda_i \rangle &= \int \rho(\lambda) d\lambda \int_0^\pi \frac{1}{\pi} \frac{d\theta}{1 + \left(R\theta e^{\frac{\lambda_i + \lambda}{\beta}}\right)^\beta} \\ &= \frac{1}{\pi R} e^{-\frac{\lambda_i}{\beta}} \langle e^{-\frac{\lambda}{\beta}} \rangle \mathcal{I}_\beta, \end{aligned} \tag{A5}$$

where $\mathcal{I}_\beta = \frac{\pi}{\beta \sin(\pi/\beta)}$ [39]. Since $\deg_i = \sum_j a_{ij}$, one finds

$$\kappa_i = \langle \deg_i \mid \lambda_i \rangle = N \langle p_{ij} \mid \lambda_i \rangle = 2\delta e^{-\frac{\lambda_i}{\beta}} \langle e^{-\frac{\lambda}{\beta}} \rangle \mathcal{I}_\beta \tag{A6}$$

and, by further integrating over λ_i, one gets $\langle e^{-\frac{\lambda}{\beta}} \rangle = \sqrt{\langle \kappa \rangle (2\delta \mathcal{I}_\beta)^{-1}}$, so that

$$e^{-\frac{\lambda_i}{\beta}} = \frac{\kappa_i}{\sqrt{\langle \kappa \rangle}} \frac{1}{\sqrt{2\delta \mathcal{I}_\beta}}. \tag{A7}$$

Plugging Eq. (A7) into Eq. (A4), one finally finds

$$p_{ij} = \frac{1}{1 + \left(\frac{x_{ij}}{\frac{\kappa_i \kappa_j}{\langle \kappa \rangle} \frac{1}{2\delta \mathcal{I}_\beta}}\right)^\beta} = \frac{1}{1 + \left(\frac{x_{ij}}{\kappa_i \kappa_j \mu}\right)^\beta}, \tag{A8}$$

where $\mu = \frac{1}{2\delta \mathcal{I}_\beta \langle \kappa \rangle}$.

In the following, it will be useful to rewrite Eq. (1) in a slightly different way. Let $M = \frac{1}{2} \sum_i \kappa_i = \frac{N}{2} \langle \kappa \rangle$ be the expected number of edges in the graph, and let $f_i = \frac{\kappa_i}{2M}$ be the normalized hidden degree of v_i, a measure of the *relative popularity* of v_i with respect to the rest of the network. Note that f_i can be interpreted as the probability that a random edge is incident on v_i, and that $\sum_i f_i = 1$. Since $x_{ij} = R\Delta(\theta_i, \theta_j)$ and $\delta = \frac{N}{2\pi R}$, Eq. (1) can be rewritten as

$$p_{ij} = \frac{1}{1 + \left(\frac{\Delta(\theta_i, \theta_j) \mathcal{I}_\beta}{2\pi M f_i f_j}\right)^\beta}. \tag{A9}$$

Equation (A9) clarifies that, for fixed M, p_{ij} decreases with the angular distance between v_i and v_j, and increases with the two nodes' popularity. In particular, the term $2Mf_if_j$ is the expected number of edges between v_i and v_j.

APPENDIX B: THE RHBM MODEL

Let the vertex set V be partitioned into n blocks $B_0, \ldots, B_{n-1}$, with $i \in I$ meaning that vertex v_i belongs to block B_I, and N_I being the size of block B_I. Let $K = \{K_{IJ}\}$ be a symmetric matrix. To each node v_i we assign a latent angular coordinate θ_i and a latent *fitness* f_i such that $\sum_{i \in I} f_i = 1$. The RHBM model is defined as the maximum-entropy probability distribution P, over the set of graphs having vertex set V, satisfying

$$\langle E \rangle_P = E^*, \tag{B1}$$

$$\langle L_{IJ} \rangle_P = K_{IJ} \quad \text{for all } I, J, \tag{B2}$$

$$\langle \deg_i \rangle_P = f_i \sum_J K_{I,J} \quad \text{for all } i, \tag{B3}$$

where, as in Sec. II, $E = \sum_{i<j} \varepsilon_{ij} a_{ij}$ is the energy of the system and $\varepsilon_{ij} = \varepsilon(x_{ij})$ is a function of the distance between v_i and v_j on the $\mathbb{S}^1$ ring.

As for the standard $\mathbb{S}^1$ model, the maximum-entropy probability per graph factorizes in terms of independent probabilities per link—this happens every time the constraints are linear in a_{ij}—as

$$p_{ij} = \frac{1}{1 + e^{\lambda_i + \lambda_j + \eta_{IJ} + \beta \varepsilon_{ij}}},$$

where $i \in I$, $j \in J$, and β, η_{IJ} and λ_i are the Lagrange multipliers associated, respectively, to conditions Eqs. (B1)–(B3). Also, with the same line of reasoning used in Ref. [34], it can be proven that taking $\varepsilon_{ij} = \ln(x_{ij})$ is the only way to suppress nonstructural degree correlations. This leads to

$$p_{ij} = \frac{1}{1 + \left(x_{ij} e^{\frac{\lambda_i + \lambda_j + \eta_{IJ}}{\beta}}\right)^\beta}. \tag{B4}$$

The latent coordinates θ_i are taken uniformly at random on $[0, 2\pi)$ with probability $\rho(\theta) = \frac{1}{2\pi}$, so that the total density of nodes on $\mathbb{S}^1$ is $\delta = \frac{N}{2\pi R}$, whereas block I has density $\delta_I = \frac{N_I}{2\pi R}$. We assume that the ratio $\frac{N_I}{N}$ stays constant as $N \to \infty$, so that $N \to \infty$ means both $R \to \infty$ and $N_I \to \infty$.

Let us consider two nodes v_i and v_j with $i \in I$ and $j \in J$. For fixed λ_i and η_{IJ} (i.e., fixed f_i and K_{IJ}), the expected

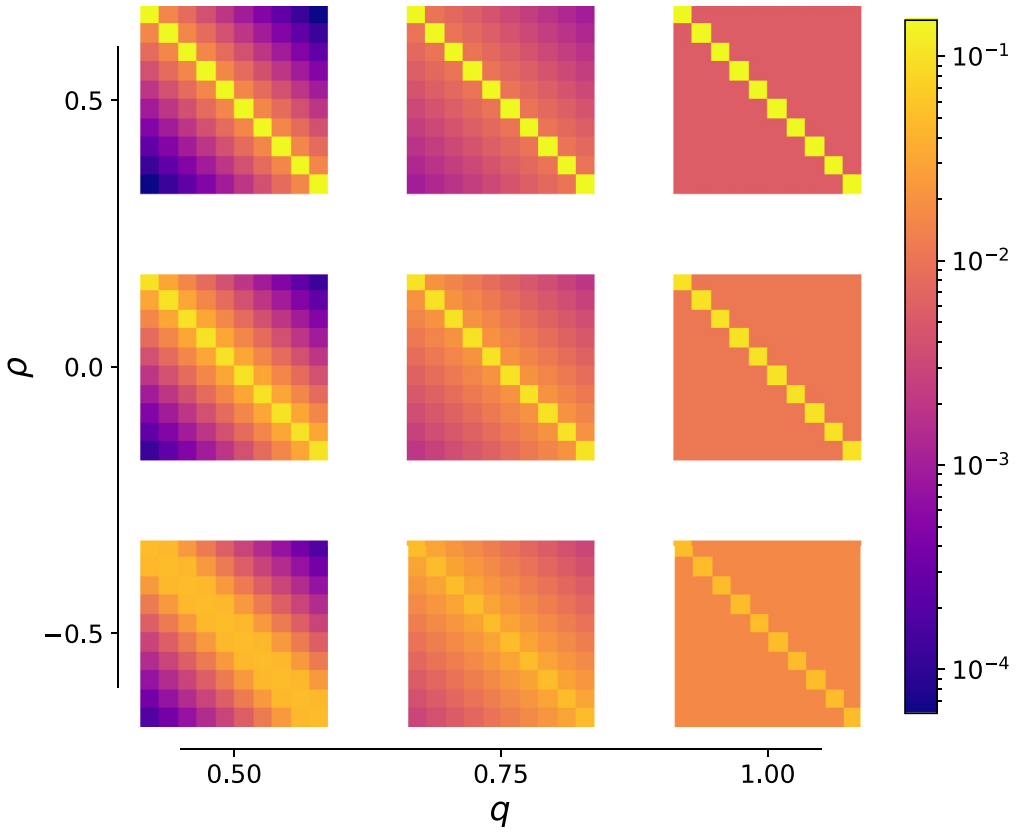

FIG. 6. A visualization of the matrix $F(q, \rho, 10)$ obtained for the considered values of q and ρ for $n = 10$ communities.

probability that v_i and v_j are connected can be found integrating p_{ij}, as a function of λ_i and η_{IJ}, over θ_j and λ_j—where, as in Appendix A, we take $\theta_i = 2\pi$ so that $\Delta(\theta_i, \theta_j) = \theta_j$:

$$\begin{aligned}\langle p_{ij} \mid \lambda_i, \eta_{IJ}, i \in I, j \in J\rangle &= \int \rho(\lambda) d\lambda \int_0^{\pi} \frac{1}{\pi} \frac{d\theta}{1 + \left(R\theta e^{\frac{\lambda_i+\lambda+\eta_{IJ}}{\beta}}\right)^{\beta}} \\ &= \frac{\mathcal{I}_\beta}{\pi R} e^{-\frac{\eta_{IJ}}{\beta}} e^{-\frac{\lambda_i}{\beta}} \langle e^{-\frac{\lambda}{\beta}}\rangle. \end{aligned} \tag{B5}$$

Since $L_{IJ} = \sum_{i\in I, j\in J} a_{ij}$, by further integrating Eq. (B5) over λ_i we obtain

$$\begin{aligned} K_{IJ} &= \langle L_{IJ} \mid \eta_{IJ}\rangle \\ &= N_I N_J \langle p_{ij} \mid \eta_{IJ}, i \in I, j \in J\rangle \\ &= N_I N_J \frac{\mathcal{I}_\beta}{\pi R} e^{-\frac{\eta_{IJ}}{\beta}} \langle e^{-\frac{\lambda}{\beta}}\rangle^2. \end{aligned} \tag{B6}$$

We can isolate $e^{-\frac{\eta_{IJ}}{\beta}}$ to obtain

$$e^{-\frac{\eta_{IJ}}{\beta}} = \frac{\pi R}{\mathcal{I}_\beta} \frac{K_{IJ}}{N_I N_J} \frac{1}{\langle e^{-\frac{\lambda}{\beta}}\rangle^2}. \tag{B7}$$

Similarly, since $\deg_i = \sum_j a_{ij} = \sum_J \sum_{j\in J} a_{ij}$, by plugging Eq. (B7) into Eq. (B5) we obtain

$$\begin{aligned} f_i \sum_J K_{I_i J} &= \langle \deg_i \mid \lambda_i, K, i \in I\rangle \\ &= \sum_J N_J \langle p_{ij} \mid \lambda_i, K_{IJ}, i \in I, j \in J\rangle \\ &= \frac{e^{-\frac{\lambda_i}{\beta}}}{\langle e^{-\frac{\lambda}{\beta}}\rangle} \frac{1}{N_I} \sum_J K_{IJ}. \end{aligned} \tag{B8}$$

If we isolate $e^{-\frac{\lambda_i}{\beta}}$, we obtain

$$e^{-\frac{\lambda_i}{\beta}} = f_i N_I \langle e^{-\frac{\lambda}{\beta}}\rangle. \tag{B9}$$

Finally, recalling that $x_{ij} = R\Delta(\theta_i, \theta_j)$ and $\delta = \frac{N}{2\pi R}$, we plug Eqs. (B7) and (B9) in Eq. (B4) to find

$$p_{ij} = \frac{1}{1 + \left(\frac{\Delta(\theta_i,\theta_j)\mathcal{I}_\beta}{\pi K_{IJ} f_i f_j}\right)^{\beta}}. \tag{B10}$$

Equation (B10) has the same functional form of Eq. (A9), with the only difference that the fitness scores f_i are now normalized *per block* and that the number of edges stubs $2M$ in Eq. (A9) is replaced by K_{IJ} in Eq. (B10).

The RHBM model as the union of $\binom{n}{2}$ $\mathbb{S}^1$ models

The RHBM model can be equivalently obtained imposing that the fitness score f_i, instead of just controlling v_i's expected *total* degree, controls v_i's expected degree towards

all blocks in the graph. This approach was recently proposed in Ref. [36], with a model that the authors denoted the hidden-degree geometric block model (HGBM). In practice, this means formulating the following system of *stronger* conditions:

$$\langle E\rangle_P = E^*, \tag{B11}$$

$$\left\langle \deg_i^J \right\rangle_P = f_i K_{IJ} \quad \text{for all } i, J, \tag{B12}$$

for given $K = \{K_{IJ}\}$ and f_i such that $\sum_{i\in I} f_i = 1$, where $\deg_i^J = \sum_{j\in J} a_{ij}$ is the number of nodes in block J to which v_i is connected.

Let us highlight that Eq. (B12) implies both Eqs. (B2) and (B3):

$$\langle L_{IJ}\rangle_P = \sum_{i\in I}\langle \deg_i^J\rangle_P = \sum_{i\in I} f_i K_{IJ} = K_{IJ},$$
$$\langle \deg_i\rangle_P = \sum_{J}\langle \deg_i^J\rangle_P = \sum_{J} f_i K_{IJ} = f_i \sum_{J} K_{IJ}.$$

The inverse is not true in general, but it is true under the maximum-entropy assumption. In fact, the maximum-entropy probability per graph factorizes in terms of independent probabilities per link as

$$p_{ij} = \frac{1}{1+e^{\lambda_{iJ}+\lambda_{jI}+\beta\varepsilon_{ij}}} \quad \text{if } i \neq j, 0 \text{ otherwise},$$

where β and λ_{iJ} are the Lagrange multipliers associated, respectively, to conditions Eqs. (B11) and (B12).

It is easy to verify that this model is equivalent to the union of the $\binom{n}{2}$ graphs obtained imposing

$$\langle E_{IJ}\rangle_P = E^*_{IJ}, \tag{B13}$$

$$\left\langle \deg_i^J \right\rangle_P = f_i K_{IJ} \quad \text{for all } i \in I, \tag{B14}$$

$$\left\langle \deg_j^I \right\rangle_P = f_j K_{IJ} \quad \text{for all } j \in J, \tag{B15}$$

for all possible choices of I, J and suitable E^*_{IJ}, where conditions (B13)–(B15) define a bipartite graph if $I \neq J$.

Based on the literature (see, e.g., Ref. [34] for the $\mathbb{S}^1$ model and Ref. [40] for the bipartite $\mathbb{S}^1 \times \mathbb{S}^1$ model), we can formulate the following probability per link:

$$p_{ij} = \frac{1}{1+\left(\frac{x_{ij}\mathcal{I}_\beta}{f_i K_{IJ} f_j K_{IJ}\frac{\pi R}{K_{IJ}}}\right)^\beta} = \frac{1}{1+\left(\frac{\Delta(\theta_i,\theta_j)\mathcal{I}_\beta}{\pi K_{IJ} f_i f_j}\right)^\beta}. \tag{B16}$$

Equation (B16) coincides with Eq. (B10), showing the equivalence of the two models. In particular, this implies that the $\mathbb{S}^1$ model can be generalized to accommodate a community structure by simply considering each subgraph as a mono/bipartite $\mathbb{S}^1$ graph, provided that

(i) the hidden degrees are replaces with hidden *fitnesses,*

(ii) both the hidden fitness f_i and the latent angular coordinate θ_i associated to vertex v_i are drawn just once and for all—i.e., not redrawn for each subgraph.

The fact that v_i has the same f_i in all subgraphs guarantees that Eq. (B3) holds and that G has, in good approximation, the desired degree distribution. On the other hand, the fact that v_i has the same θ_i in all subgraphs preserves the transitivity of the vertex similarity across different subgraphs, so as to guarantee the desired high clustering for the entire graph.

APPENDIX C: PARAMETRIC NETWORK MODEL USED IN EXPERIMENTS

Equation (17), that defines the parametric model used to generate matrices for our experiments, can be rewritten more explicitly as

$$F(q,\rho,n) = \frac{1+\rho}{n}\begin{bmatrix} 1 & 0 & 0 & \cdots & 0 \\ 0 & 1 & 0 & \cdots & 0 \\ 0 & 0 & 1 & \cdots & 0 \\ \vdots & & & \ddots & \\ 0 & 0 & 0 & \cdots & 1 \end{bmatrix} + \frac{1-\rho}{2\sum_{i=1}^{n}(n-i)q^i}\begin{bmatrix} 0 & q & q^2 & \cdots & q^{n-1} \\ q & 0 & q & \cdots & q^{n-2} \\ q^2 & q & 0 & \cdots & q^{n-3} \\ \vdots & & & \ddots & \\ q^{n-1} & q^{n-2} & q^{n-3} & \cdots & 0 \end{bmatrix}.$$

Figure 6 shows some of these matrices, as a function of q and ρ, for the case of $n = 10$ communities. While not intended to be an exhaustive representation of real-world mixing patterns, these matrices capture a significant range of realistic structural schemes observed in empirical data.

[1] J. S. Archana and M. R. Kaimal, Community detection in complex networks using randomisation, in *Proceedings of the 2014 International Conference on Interdisciplinary Advances in Applied Computing (ICONIAAC '14)*, Vol. 32 (Association for Computing Machinery, New York, NY, 2014), pp. 1–5.

[2] M. Salathé and J. H. Jones, Dynamics and control of diseases in networks with community structure, PLoS Comput. Biol. **6**, e1000736 (2010).

[3] A. Celestini, F. Colaiori, S. Guarino, E. Mastrostefano, and L. R. Zastrow, Epidemics in a synthetic urban population with multiple levels of mixing, in *International Conference on Complex Networks and Their Applications* (Springer, 2021), pp. 315–326.

[4] C. I. Del Genio, T. Gross, and K. E. Bassler, All scale-free networks are sparse, Phys. Rev. Lett. **107**, 178701 (2011).

[5] D. J. Watts and S. H. Strogatz, Collective dynamics of 'small-world'networks, Nature (London) **393**, 440 (1998).

[6] A.-L. Barabási and R. Albert, Emergence of scaling in random networks, Science **286**, 509 (1999).

[7] D. Krioukov, Clustering implies geometry in networks, Phys. Rev. Lett. **116**, 208302 (2016).

[8] R. Toivonen, J.-P. Onnela, J. Saramäki, J. Hyvönen, and K. Kaski, A model for social networks, Physica A **371**, 851 (2006).

[9] M. Girvan and M. E. Newman, Community structure in social and biological networks, Proc. Natl. Acad. Sci. **99**, 7821 (2002).

[10] H. Cherifi, G. Palla, B. K. Szymanski, and X. Lu, On community structure in complex networks: Challenges and opportunities, Appl. Network Sci. **4**, 117 (2019).

[11] D. Krioukov, F. Papadopoulos, M. Kitsak, A. Vahdat, and M. Boguñá, Hyperbolic geometry of complex networks, Phys. Rev. E **82**, 036106 (2010).

[12] K. Zuev, M. Boguná, G. Bianconi, and D. Krioukov, Emergence of soft communities from geometric preferential attachment, Sci. Rep. **5**, 9421 (2015).

[13] B. Kovács and G. Palla, The inherent community structure of hyperbolic networks, Sci. Rep. **11**, 16050 (2021).

[14] M. A. Serrano and M. Boguná, The shortest path to network geometry: A practical guide to basic models and applications, elements in *Structure and Dynamics of Complex Networks* (Cambridge University Press, Cambridge, England, 2022).

[15] M. Boguñá, F. Papadopoulos, and D. Krioukov, Sustaining the internet with hyperbolic mapping, Nat. Commun. **1**, 62 (2010).

[16] A. Muscoloni and C. V. Cannistraci, Angular separability of data clusters or network communities in geometrical space and its relevance to hyperbolic embedding, arXiv:1907.00025.

[17] W. Yang and D. Rideout, High dimensional hyperbolic geometry of complex networks, Mathematics **8**, 1861 (2020).

[18] F. Papadopoulos, M. Kitsak, M. Serrano, M. Boguná, and D. Krioukov, Popularity versus similarity in growing networks, Nature (London) **489**, 537 (2012).

[19] A. Muscoloni and C. V. Cannistraci, A nonuniform popularity-similarity optimization (nPSO) model to efficiently generate realistic complex networks with communities, New J. Phys. **20**, 052002 (2018).

[20] G. García-Pérez, M. Á. Serrano, and M. Boguñá, Soft communities in similarity space, J. Stat. Phys. **173**, 775 (2018).

[21] Z. Wang, Q. Li, F. Jin, W. Xiong, and Y. Wu, Hyperbolic mapping of complex networks based on community information, Physica A **455**, 104 (2016).

[22] A. Faqeeh, S. Osat, and F. Radicchi, Characterizing the analogy between hyperbolic embedding and community structure of complex networks, Phys. Rev. Lett. **121**, 098301 (2018).

[23] R. Jankowski, A. Allard, M. Boguñá, and M. Á. Serrano, The d-mercator method for the multidimensional hyperbolic embedding of real networks, Nat. Commun. **14**, 7585 (2023).

[24] M. Bruno, S. F. Sousa, F. Gursoy, M. Serafino, F. V. Vianello, A. Vranić, and M. Boguñá, Community detection in the hyperbolic space, arXiv:1906.09082.

[25] D. Ye, H. Jiang, Y. Jiang, Q. Wang, and Y. Hu, Community preserving mapping for network hyperbolic embedding, Knowl.-Based Syst. **246**, 108699 (2022).

[26] S. Talaga and A. Nowak, Structural measures of similarity and complementarity in complex networks, Sci. Rep. **12**, 16580 (2022).

[27] G. Budel and M. Kitsak, Complementarity in complex networks, arXiv:2003.06665.

[28] G. Budel, Y. Jin, P. Van Mieghem, and M. Kitsak, Topological properties and organizing principles of semantic networks, Sci. Rep. **13**, 11728 (2023).

[29] P. Almagro, M. Boguñá, and M. Á. Serrano, Detecting the ultra low dimensionality of real networks, Nat. Commun. **13**, 6096 (2022).

[30] B. Kovács, S. G. Balogh, and G. Palla, Generalised popularity-similarity optimisation model for growing hyperbolic networks beyond two dimensions, Sci. Rep. **12**, 968 (2022).

[31] G. Budel, M. Kitsak, R. Aldecoa, K. Zuev, and D. Krioukov, Random hyperbolic graphs in $d+1$ dimensions, Phys. Rev. E **109**, 054131 (2024).

[32] B. Désy, P. Desrosiers, and A. Allard, Dimension matters when modeling network communities in hyperbolic spaces, PNAS Nexus **2**, pgad136 (2023).

[33] G. García-Pérez, M. Boguñá, and M. Á. Serrano, Multiscale unfolding of real networks by geometric renormalization, Nat. Phys. **14**, 583 (2018).

[34] M. Boguñá, D. Krioukov, P. Almagro, and M. A. Serrano, Small worlds and clustering in spatial networks, Phys. Rev. Res. **2**, 023040 (2020).

[35] In the following, we use lower-case indices for nodes and upper-case indices for blocks, with $i \in I$ indicating that node i belongs to block I, and I_i denoting i's block.

[36] S. Guarino, E. Mastrostefano, and D. Torre, The hidden-degree geometric block model, in *International Conference on Complex Networks and Their Applications* (Springer, 2023), pp. 409–419.

[37] T. P. Peixoto, Nonparametric bayesian inference of the microcanonical stochastic block model, Phys. Rev. E **95**, 012317 (2017).

[38] https://gitlab.com/s.guarino/geometric_block_model.

[39] The right-hand side. of Eq. (A5) follows from $\frac{1}{X}\int_0^X \frac{dt}{1+t^\beta} \overset{X\to\infty}{\approx} \frac{\pi}{\beta\sin(\pi/\beta)}\cdot\frac{1}{X} = \frac{\mathcal{I}_\beta}{X}$ and the fact that $N\to\infty$ means $R\to\infty$ for fixed δ. In Eq. (A5), $\rho(\lambda)$ is the density over λ induced by $\rho(\kappa)$.

[40] M. Kitsak, F. Papadopoulos, and D. Krioukov, Latent geometry of bipartite networks, Phys. Rev. E **95**, 032309 (2017).